Dynamic Compression of Single Nanochannel Confined DNA via a Nanodozer Assay

Ahmed Khorshid,[1] Philip Zimny,[1] David Tétreault-La Roche,[1] Geremia Massarelli,[1] Takahiro Sakaue,[2,*] and Walter Reisner[1,†]

[1]*Department of Physics, McGill University, 3600 rue university, Montreal, Quebec H3A 2T8, Canada*

[2]*Department of Physics, Kyushu University 33, Fukuoka 812-8581, Japan*

(Received 13 August 2014; revised manuscript received 23 October 2014; published 30 December 2014)

We show that a single DNA molecule confined and extended in a nanochannel can be dynamically compressed by sliding a permeable gasket at a fixed velocity relative to the stationary polymer. The gasket is realized experimentally by optically trapping a nanosphere inside a nanochannel. The trapped bead acts like a "nanodozer," directly applying compressive forces to the molecule without requirement of chemical attachment. Remarkably, these strongly nonequilibrium measurements can be quantified via a simple nonlinear convective-diffusion formalism and yield insights into the local blob statistics, allowing us to conclude that the compressed nanochannel-confined chain exhibits mean-field behavior.

DOI: 10.1103/PhysRevLett.113.268104 PACS numbers: 87.14.gk, 82.35.Lr, 82.37.Rs, 87.15.H-

Experiment, simulation, and scaling analytics are converging on a comprehensive picture regarding the *equilibrium* behavior of nanochannel-confined semiflexible, self-avoiding chains [1]. Yet, strongly *nonequilibrium* behavior of confined polymers is largely unexplored from either an experimental or theoretical point of view. From the perspective of applications, quantifying nonequilibrium behavior is essential to overcoming a variety of technical challenges related to nanochannel DNA mapping [2,3], including the entry of polymers into nanochannels, interaction with defects [4], and modeling chain relaxation [5]. In particular, there is a need for experimentally validated models that can predict how confined and highly concentrated DNA evolves in time and space [6–8] (e.g., to model entropic trap arrays [9,10] and elucidate biophysical problems ranging from the viral ejection of DNA into cells to chromosomal dynamics [11]).

In this Letter a sliding gasket is used to dynamically compress single nanochannel confined double-stranded DNA (see Fig. 1). The gasket is realized via our "nanodozer assay": a bead is optically trapped inside the nanochannel with a diameter that is a large fraction of the channel width; a nanostage is then used to translate the nanofluidic device at a fixed trap position, sliding the bead relative to the DNA molecule with a speed V. By varying V over 2 orders of magnitude (0.1–10 μm/s), we deduce the dynamic response of single nanochannel confined polymers to forcing conditions ranging from near equilibrium to strongly out of equilibrium. We find that the dynamically forced chains will undergo transient dynamics and reach a well-defined highly compressed steady state. This steady-state behavior is characterized by a time-invariant average extension r and a concentration profile $c_S(x)$ (units of chain contour per unit channel length). The concentration profile, according to a blob-based model we introduce, encodes information relating to the local blob statistics, allowing us to discriminate between fluctuating and mean-field descriptions of the compressed chain. Moreover, we observe distinct dynamical compression regimes, separated by a critical speed V_c, in agreement with the blob model predictions. While electric and hydrodynamic forcing has been used to compress DNA against barriers in nanochannels [4,5], these experiments were relatively uncontrolled and it was not possible to quantify chain dynamic response as a function of applied forcing (as demonstrated here). J. Pelletier *et al.* [11] used an optically trapped bead inside a microchannel (1 μm in diameter) to compress an *E. coli* chromosome against a barrier formed by a blunt ended channel, but this study focused on equilibrium compression and did not explore the dynamic regimes described here.

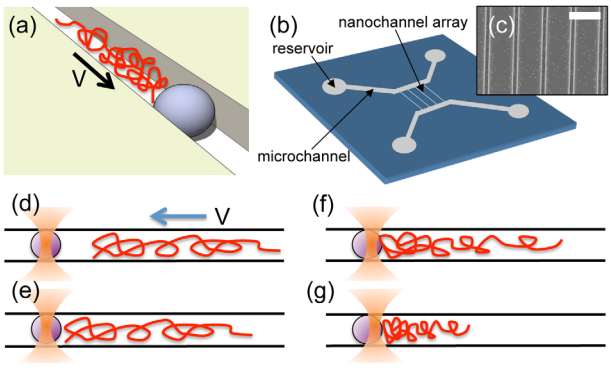

FIG. 1 (color online). (a) A 3D graphic of a bead gasket initiating compression of a nanochannel-confined polymer molecule. (b) The device geometry: an array of nanochannels spans the gap between two U-shaped microchannels. The microchannels, used to load DNA and beads into the nanochannels, are coupled to four reservoirs that contain sandblasted loading ports. (c) An SEM of the 300 × 310 nm nanochannels used in the study (2 μm scale bar). (d)–(g) A graphical compression event, shown in the frame comoving with the bead.

The nanochannels used were fabricated in fused silica wafers (HOYA) using the protocol described in Ref. [1]. The channels have a dimension of $\sim 300 \times 310$ nm, as obtained from SEM imaging and surface profilometry. The chips were directly bonded to fused silica coverslips to form all silica channels. The devices were wet with a buffer consisting of a 10 mM tris buffer at pH 8.0. Compression experiments were conduced with T_4 bacteriophage DNA (Nippon Gene, 166 kbp) stained with YOYO-1 at an intercalation ratio of 10:1, leading to a total contour length of roughly 63.7 μm [12]. The mean equilibrium extension of nanochannel-confined T_4 is $r_0 = 14.5 \pm 0.3$ μm. The nanogaskets were formed using fluorescent 200 nm polystyrene beads (Duke Scientific). The devices were incubated for 24 h in 8% PVP-10 (Polyvinylpyrrolidone, Sigma-Aldrich) to prevent the sticking of beads to channel surfaces. In addition, β-mercaptoethanol at 2% was added as an antinicking and bleaching agent. Our optical setup was based on a iXon EMCCD camera (Andor) mounted on a Nikon Eclipse Ti microscope using a $100 \times$ N.A. 1.5 oil immersion objective (Nikon). A metal-halide lamp was used as an excitation source (Xcite). The optical trap was formed around a 1064 nm laser (Crystal Laser), expanded and introduced into the back-focal aperture of the objective. The device is moved with respect to a fixed trap position via a combined micro- (Prior) and nanostage (Mad City).

The T_4 DNA is driven from the microchannels into the nanochannel array by pneumatic pressure created via a steady N_2 flow applied at the reservoir. The optical trap is then used to capture a single 200 nm bead from the microchannels and introduce the bead into a DNA containing nanochannel. In certain cases, multiple beads are trapped simultaneously to avoid DNA slippage through the gasket at high compression speeds. Once the bead is brought into proximity of a given DNA, the nanostage affects a one-dimensional translation driving the DNA against the bead at speed V. The nanostage translation is started a few seconds after recording begins in order to obtain a measurement of the molecule equilibrium extension r_0 and average equilibrium intensity I_0. In order to view the compression event in its entirety, we transform the image series into a kymograph representation by reslicing so that time is displayed along the x axis and nanochannel position along the y axis [see Fig. 2(e)]. As the bead comes into contact with the DNA, it starts deforming in the bead's immediate vicinity, undergoing a transient compression before reaching a final steady state. The steady-state concentration profile $c_s(x)$ of the nanochannel-confined polymer (units of contour per unit volume), proportional to the local fluorescence, can be measured by averaging the frames taken over the steady portion of the kymograph [see inset of Fig. 2(f)]. In order to remove the intensity profile of the bead, the bead's intensity profile is obtained independently from frames taken prior to collision and then subtracted from the profile [see Fig. 2(f)]. The steady-state

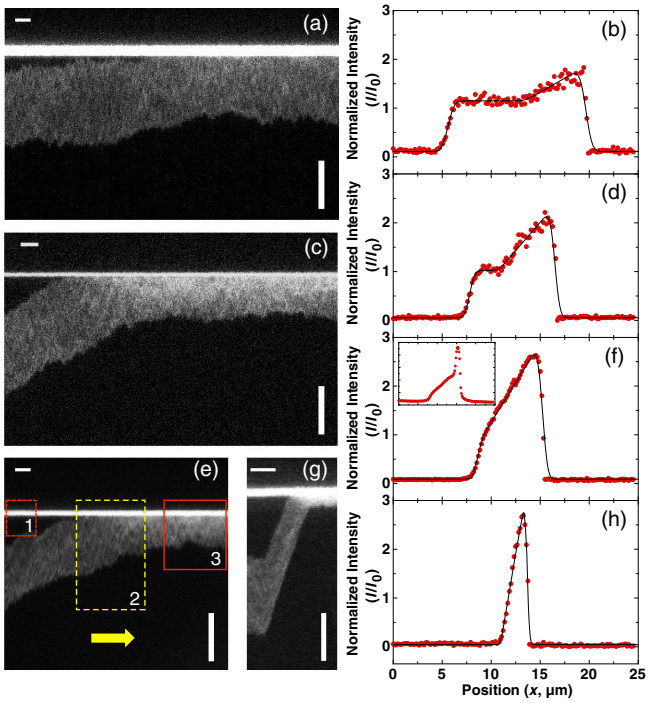

FIG. 2 (color online). (a),(b) and (c),(d) and (e),(f) and (g),(h), respectively, show kymographs and corresponding steady-state ramp profiles with linear ramp fits for compression events with $V = 0.1$ μm/s [(a),(b)], 0.25 μm/s [(c),(d)], 1 μm/s [(e),(f)], and 10 μm/s [(g),(h)]. The vertical scale bar is 10 μm; the horizontal bar gives a time scale of 2 s capturing compression events progressing from left to right. (a),(b) is a compression event at a very low V where the molecule is slightly compressed and translocating close to its equilibrium state. Note that profiles (a), (b) and (c),(d) exist in regime II. The boxes on (e) snapshot (1) bead intensity, (2) transient dynamics, and (3) steady-state regime. The inset in (f) shows the intensity profile prior to bead subtraction.

profile is then normalized to I_0: note that $I(x)/I_0 = c(x)/c_0$. Figure 2 shows representative kymographs and steady-state profiles for compression events taken for four different sliding speeds. For the very lowest speeds ($< 0.5\,\mu$m/s), we observe steady-state profiles that contain a "flat" portion at the equilibrium concentration connected to a ramp-type profile [Figs. 2(b) and 2(d)]. For higher speeds we observe only ramp-type profiles [Figs. 2(f) and 2(h)]. The ramp profile is well fit to a linear model [Figs. 2(b), 2(d), 2(f), and 2(h)] with a slope or "ramp rate" scaling linearly with V [Fig. 3(a)].

In addition to the ramp rate we can extract the dynamic chain extension (r) and the intensity measured at the molecule edge opposite the bead normalized to I_0 (f_{edge}). In order to extract these quantities from the intensity profiles, we must take into account that the measured ramp profile, assumed to have a linear form, is in fact the convolution of the true DNA intensity profile with the optical point-spread function, represented as a Gaussian function with a standard deviation of σ. The convolution

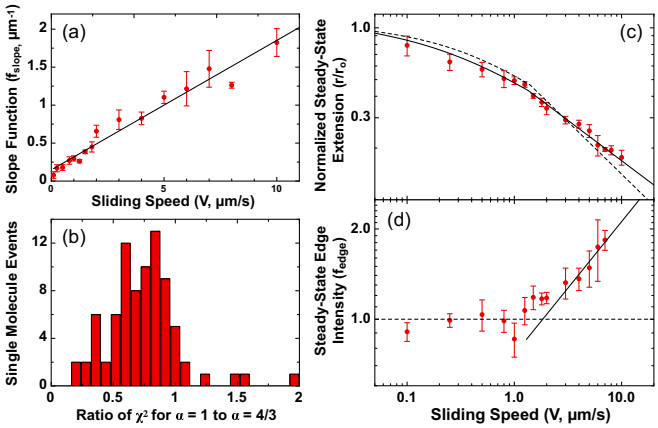

FIG. 3 (color online). (a) The slope function f_{slope} versus sliding speed with a linear least-squares fit. The best-fit slope $A_{\mathrm{slope}} = 0.17 \pm 0.01$ s/μm^2. (b) Histogrammed values of the χ^2 ratio for fits to the experimental intensity profiles with $\alpha = 1$ and $\alpha = 4/3$. The mean value of the χ^2 ratio is 0.74 ± 0.03, strong evidence that $\alpha = 1$ is correct. (c) The steady-state extension r_{min}/r_0 as a function of sliding speed with a least-squares fit (the bold line) to the combined blob model prediction for regime II and III, yielding $\beta = 0.48 \pm 0.2$ and a self-consistently determined $V_c = 1.4 \pm 0.5$ μm/s. The prediction for $\beta = 4/7$ ($\nu = 3/5$) is shown for comparison (the dashed curve). (d) The steady-state edge intensity: the edge intensity is consistent with unity (the dashed line) for $V < V_c$ and then rises monotonically. A power-law fit (the bold line) to the high-V points ($V > 2$ μm/s) yields $\gamma = 0.44 \pm 0.15$.

can be performed analytically, leading to a fitting function that enables the self-consistent extraction of r and f_{edge}. The extension r as a function of V is shown in Fig. 3(c). The r versus V data appear to follow a power law ($V \sim V^{\beta}$) for speeds above a critical speed V_c (in the range of 1–2 μ/s). For speeds below V_c the chain is only weakly compressed and rises to r_0 as V approaches zero. The normalized edge intensity is flat and consistent with unity for $V < V_c$ and rises above unity for $V > V_c$ [Fig. 3(d)]. The distinct behaviors of r and f_{edge} above and below V_c suggest that V_c may demarcate two different dynamical regimes.

In order to gain a more quantitative insight into the compression phenomena, we introduce a dynamical blob-based model [6]. The bead-DNA interaction is most conveniently modeled by working in the frame of reference moving with the bead (gasket), in which we assume the molecule, of contour length L, feels a uniform flow of speed V compressing it against the gasket but does not translate [Fig. 4(a)]. Let $x = 0$ denote the edge of the chain away from the bead and let $x = r$ denote the molecule edge facing the bead (gasket). A blob at position x, for channels in our size range, will feel a drag force $f_{\mathrm{drag}} \simeq \eta x V$ [13] and will start to deform when $f_{\mathrm{drag}} \simeq k_B T/D$ [14]. The drag force is necessarily highest for the blob facing the gasket (i.e., at $x = r$): this blob will be the first to deform as the speed is increased from zero, initiating compression of the

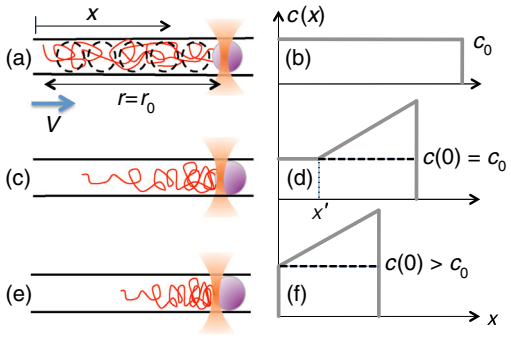

FIG. 4 (color online). (a) A graphic and (b) a schematic of the steady-state concentration profile $c_s(x)$ for sliding speeds $V < V^{\star}$ (regime I): in this regime the polymer translates with the bead. (c) A graphic and (d) a schematic of $c_s(x)$ for sliding speeds $V^{\star} < V < V^{\star\star}$ (regime II): in this regime the polymer is partially compressed. (e) A graphic and (f) a schematic of $c_s(x)$ for $V > V^{\star\star}$ (regime III): in this regime the polymer is entirely compressed.

chain. In fact, this blob will deform at a speed $V^{\star}$ satisfying $\eta r_0 V^{\star} \simeq k_B T/D$. For speeds $V < V^{\star}$, the chain will slide down the channel at its equilibrium extension $r = r_0$ [regime I, Figs. 4(a) and 4(b)]. For speeds $V > V^{\star}$ the chain will compress, but only partially [regime II, Figs. 4(c) and 4(d)], leaving a portion of the chain at the constant equilibrium concentration $c_0 = L/r_0$. The junction between the compressed and unaltered portions of the chain occurs at $x' \simeq DV^{\star\star}/V$, where $V^{\star\star} = k_B T/D^2\eta$ is a characteristic velocity in the channel. As the sliding speed is increased still further, the blob at $x = 0$ eventually deforms, at which point the entire chain will be compressed [regime III, Figs. 4(e) and 4(f)]. This happens at $V^{\star\star}$, for which $\eta D V^{\star\star} = k_B T/D$.

The steady state is reached when the convective current of polymer contour cV balances the diffusional current $D_c(\partial c/\partial x)$ [6]:

$$D_c \frac{\partial c}{\partial x} = cV. \tag{1}$$

The quantity D_c is a cooperative diffusion coefficient and is itself a function of chain concentration, determined via the local blob statistics by $D_c = k_B T/\eta\xi$, with η representing the viscosity and ξ the blob size [6,15]. The blob size is given in terms of N_b, the number of Kuhn lengths per blob by $\xi \sim N_b^{\nu}$. If the blobs are ideal, $\nu = 1/2$; this corresponds to a mean-field regime. If the blobs exhibit Flory scaling, $\nu = 3/5$; this corresponds to classic fluctuating semidilute solution behavior [16,17]. We disregard throughout the Letter subtle dependences on the segment aspect ratio $\epsilon = w/P$ [18] (with w being the effective segment thickness, P the persistence length), and we focus on the most robust feature associated with the exponent ν, which dictates the local blob statistics. If we envision the confined polymer as consisting of a uniform packing of blobs

TABLE I. Values of dynamical exponents in convective-diffusion formalism. (1) α is the profile exponent. (2) The steady state $r \sim V^{-\beta}$ for $V \gg V^{\star\star}$. (3) $c(0) \sim V^{\gamma}$ and $D_{\mathrm{diff}} \sim c^{\delta}$.

Exponent	ν	$\nu = 1/2$	$\nu = 3/5$
α	$\frac{3\nu-1}{\nu}$	1	4/3
β	$\frac{3\nu-1}{4\nu-1}$	1/2	4/7
γ	$\frac{3\nu-1}{2\nu}$	1/2	2/3
δ	$\frac{\nu}{3\nu-1}$	1	3/4

[16,18], we find $\xi \sim c^{-\delta}$, with $\delta = (\nu/3\nu - 1)$ (see Table I for values of δ for blobs with ideal and Flory scaling).

Equation (1) can be integrated to obtain the steady-state concentration profile once the concentration at the ramp edge is specified. Here we discuss only the results of the model (see the Supplemental Material [19] for full details). The regime III concentration profile, with $\mu \equiv V/V^{\star\star}$, is

$$c_S(x)/c_0 = f_{\mathrm{edge}}(\mu)\left(1 + \frac{f_{\mathrm{slope}}(\mu)}{f_{\mathrm{edge}}^{1/\alpha}(\mu)}x\right)^{\alpha}. \qquad (2)$$

The profile exponent $\alpha = 1/\delta$. The edge function f_{edge} determines the chain concentration at the molecule edge opposite the gasket (relative to c_0): $f_{\mathrm{edge}}(\mu) = \mu^{\gamma}$ for $\mu \geq 1$ and $f_{\mathrm{edge}}(\mu) = 1$ for $\mu < 1$. The slope function f_{slope} determines the V dependence of the profile ramp rate: $f_{\mathrm{slope}}(\mu) = A_0 D^{-1}\mu \equiv A_{\mathrm{slope}} V$ for all V. The quantity A_0 is a scaling prefactor (to be obtained from an experiment). The regime II profile is similar to Eq. (2), but contains an initial flat portion at c_0 up to the junction position x' at which $c(x') = c_0$ [Fig. 4(d); see also the Supplemental Material [19], Eq. (3)]. Finally, we note that L is fixed, so that integrating Eq. (2) and back solving yields an expression for $r(\mu)$ [see the Supplemental Material [19], Eqs. (5), (7), and (8)]. The key result is that for $V > V^{\star\star}$, $r \sim \mu^{-\beta}$, with $\beta = \alpha/(1+\alpha) = (3\nu - 1)/(4\nu - 1)$.

The blob model predictions agree extremely well with our experimental results. First, as observed, the blob model predicts at low speeds steady-state profiles consisting of a ramp jointed to a flat segment at the equilibrium concentration [appropriate for regime II, Fig. 4(d)]. At high speeds the blob model predicts a pure ramp [appropriate for regime III, Fig. 4(f)]. Second, Eq. (2) using the mean-field exponent $\alpha = 1$ is indeed consistent with the observed linear behavior of the ramps. To test further whether the ramps are linear or might be better characterized by the slightly higher fluctuating value of $\alpha = 4/3$, we computed the ratio of the χ^2 values resulting from fits of ramped profiles to Eq. (2) for $\alpha = 1$ and $\alpha = 4/3$ [Fig. 3(b)]. The mean value of the χ^2 ratio is 0.74 ± 0.03, significantly below unity and indicating that the mean-field exponent ($\alpha = 1$) describes our data best as initially assumed. Third, f_{edge} [Fig. 3(d)] exhibits behavior in agreement with the blob model: flat and consistent with unity below V_c (expected for regime II) and monotonic rising above (expected for regime III). Based on this observation, we can identify the parameter V_c, the critical speed observed on purely experimental grounds, with the theoretical characteristic speed $V^{\star\star}$ demarcating the boundary of regimes II and III. Moreover, the f_{edge} data above V_c can be fit to a power law that yields $\gamma = 0.44 \pm 0.15$, consistent with the mean-field value of $\gamma = 1/2$ predicted by the blob model. Fourth, the experimental r versus V behavior is consistent with the blob model (power law above V_c, expected for regime III, non—power law below, expected for regime II). The combined model joining together the blob picture's quantitative predictions for regimes II and III (see the Supplemental Material [19]) can be fit in the least-square sense to the entire r versus V data set [Fig. 3(c)], yielding $\beta = 0.48 \pm 0.2$ (consistent with the mean field) and $V_c = V^{\star\star} = 1.4 \pm 0.5$ μm/s. Finally, the ramp rate, as predicted, does indeed scale linearly with V for regimes II and III [Fig. 3(a)]. The fitted slope $A_{\mathrm{slope}} = 0.17 \pm 0.01$ s/μm^2, from which the scaling constant can be estimated: $A_o = 0.07 \pm 0.05$. Note that we do not reach regime I in our study: $V^{\star} = (D/r_0)V^{\star\star} \sim 0.02$ μm/s, an order of magnitude below the lowest V value used.

We believe our approach could be used to probe chain statistics over a wide range of nanochannel dimensions and varying degrees of chain compression. We might expect, for example, to observe different dynamical exponents for larger or smaller D, especially for channels approaching P where the chain statistics might deviate from blob model predictions. While, precisely speaking, our method does not probe the statistics of equilibrium (noncompressed) chains, we believe that the statistics observed under compression are related to the statistics obeyed in the equilibrium (noncompressed) regimes. In particular, it is likely that the mean-field behavior we observe is closely connected with the extended de Gennes regime [20,21] for equilibrium chains. The extended de Gennes regime has been posited on theoretical grounds but is challenging to confirm experimentally [12]. Experiments for channels $\sim P - 2P$ might give insights into the nature of the still elusive "transition regime" [1]. Moreover, the chain statistics could be a complex function of local chain compression. The chain might transition, as it is compressed, through a number of subtle confinement regimes linking the quasi-one-dimensional channel and quasi-zero-dimensional cavity cases (as has been suggested for flexible polymers [22]). Finally, the nanodozer assay could be extended beyond single polymer systems to investigate the dynamic response of multiple polymers [23], or even polymer solutions in confinement.

This work was funded through the Natural Sciences and Engineering Research Council of Canada (NSERC) Discovery Grants Program (Grant No. RGPIN 386212), the

Fonds de recherché du Québec—Nature et technologies (FQRNT) Projet d'équipe (PR-180418), KAKENHI [Grant No. 26103525, "Fluctuation and Structure" and Grant No. 24340100, Grant-in-Aid for Scientific Research (B)], Ministry of Education, Culture, Sports, Science and Technology (MEXT), Japan, and JSPS Core-to-Core Program (Nonequilibrium Dynamics of Soft Matter and Information). We also acknowledge Enhanced Education Program (EEP) in Kyushu University through which this collaboration has been initiated.

*Corresponding author.
reisner@physics.mcgill.ca
†Corresponding author.
sakaue@phys.kyushu-u.ac.jp

[1] W. Reisner, J. N. Pedersen, and R. H. Austin, Rep. Prog. Phys. **75**, 106601 (2012).
[2] W. Reisner, N. B. Larsen, A. Silahtaroglu, A. Kristensen, N. Tommerup, J. O. Tegenfeldt, and H. Flyvbjerg, Proc. Natl. Acad. Sci. U.S.A. **107**, 13294 (2010).
[3] E. T. Lam, A. Hastie, C. Lin, D. Ehrlich, S. K. Das, M. D. Austin, P. Deshpande, H. Cao, N. Nagarajan, M. Xiao, and P.-Y. Kwok, Nat. Biotechnol. **30**, 771 (2012).
[4] C. H. Reccius, J. T. Mannion, J. D. Cross, and H. G. Craighead, Phys. Rev. Lett. **95**, 268101 (2005).
[5] J. T. Mannion, C. H. Reccius, J. D. Cross, and H. G. Craighead, Biophys. J. **90**, 4538 (2006).
[6] T. Sakaue and N. Yoshinaga, Phys. Rev. Lett. **102**, 148302 (2009).
[7] T. Sakaue, T. Saito, and H. Wada, Phys. Rev. E **86**, 011804 (2012).
[8] P. Rowghanian and A. Y. Grosberg, Phys. Rev. E **86**, 011803 (2012).
[9] M. B. Mikkelsen, W. Reisner, H. Flyvbjerg, and A. Kristensen, Nano Lett. **11**, 1598 (2011).
[10] J. Han, S. W. Turner, and H. G. Craighead, Phys. Rev. Lett. **83**, 1688 (1999).
[11] J. Pelletier, K. Halvorsen, B.-Y. Ha, R. Paparcone, S. J. Sandler, C. L. Woldringh, W. P. Wong, and S. Jun, Proc. Natl. Acad. Sci. U.S.A. **109**, E2649 (2012).
[12] D. Gupta, J. Sheats, A. Muralidhar, J. J. Miller, D. E. Huang, S. Mahshid, K. D. Dorfman, and W. Reisner, J. Chem. Phys. **140**, 214901 (2014).
[13] D. R. Tree, Y. Wang, and K. D. Dorfman, Phys. Rev. Lett. **108**, 228105 (2012).
[14] F. Brochard-Wyart, Europhys. Lett. **30**, 387 (1995).
[15] P. G. de Gennes, *Scaling Concepts in Polymer Physics* (Cornell University Press, Ithaca, NY, 1979).
[16] T. Sakaue and E. Raphaël, Macromolecules **39**, 2621 (2006).
[17] S. Jun, A. Arnold, and B.-Y. Ha, Phys. Rev. Lett. **98**, 128303 (2007).
[18] T. Sakaue, Macromolecules **40**, 5206 (2007).
[19] See Supplemental Material at http://link.aps.org/supplemental/10.1103/PhysRevLett.113.268104 for detailed derivation.
[20] Y. Wang, D. R. Tree, and K. D. Dorfman, Macromolecules **44**, 6594 (2011).
[21] A. Huang and A. Bhattacharya, Europhys. Lett. **106**, 18004 (2014).
[22] S. Jun, D. Thirumalai, and B.-Y. Ha, Phys. Rev. Lett. **101**, 138101 (2008).
[23] Y. Jung, J. Kim, S. Jun, and B.-Y. Ha, Macromolecules **45**, 3256 (2012).